

Solution structure of DFF40 and DFF45 N-terminal domain complex and mutual chaperone activity of DFF40 and DFF45

Pei Zhou*, Alexey A. Lugovskoy*[†], John S. McCarty[‡], Peng Li[‡], and Gerhard Wagner*[§]

*Department of Biological Chemistry and Molecular Pharmacology, Harvard Medical School, Boston, MA 02115; [†]Committee on Higher Degrees in Biophysics, Harvard University, Cambridge, MA 02138; and [‡]Laboratory for Apoptosis Regulation, Institute of Molecular and Cell Biology, 30 Medical Drive, Singapore 117609, Singapore

Communicated by Stanley J. Korsmeyer, Dana-Farber Cancer Institute, Boston, MA, March 26, 2001 (received for review January 5, 2001)

Apoptotic DNA fragmentation is mediated by a caspase-activated DNA fragmentation factor (DFF)40. Expression and folding of DFF40 require the presence of DFF45, which also acts as a nuclease inhibitor before DFF40 activation by execution caspases. The N-terminal domains (NTDs) of both proteins are homologous, and their interaction plays a key role in the proper functioning of this two-component system. Here we report that the NTD of DFF45 alone is unstructured in solution, and its folding is induced upon binding to DFF40 NTD. Therefore, folding of both proteins regulates the formation of the DFF40/DFF45 complex. The solution structure of the heterodimeric complex between NTDs of DFF40 and DFF45 reported here shows that the mutual chaperoning includes the formation of an extensive network of intermolecular interactions that bury a hydrophobic cluster inside the interface, surrounded by intermolecular salt bridges.

Apoptosis, a morphologically distinct form of programmed cell death plays an essential part in cell development, tissue homeostasis, and defense against pathogens. The malfunction of apoptotic machinery is intricately linked to cancer and neurodegenerative diseases (1). DNA fragmentation, triggered by nuclease DNA fragmentation factor (DFF)40, is a characteristic event of the late stage of apoptosis (2–5). In normal cells, the activity of DFF40 is completely inhibited by its binding to DFF45. These proteins share a homologous N-terminal domain (NTD) that has been termed the “cell-death inducing DFF45-like effector” (CIDE) domain and is conserved within CIDE family proteins (Fig. 1; refs. 6–8). The formation of the DFF40/DFF45 heterodimeric complex is achieved through synergistic interactions between the N-terminal and C-terminal domains of these proteins (9). Apoptotically activated execution caspases (e.g., caspase-3) cleave DFF45 into three fragments which dissociate from DFF40 and release nuclease DFF40 from its inhibited state. Caspase-3-activated DFF40 degrades nucleosomal DNA into fragments of ≈ 200 base pairs (2, 4). It has been postulated that DFF40 is active as an oligomer interacting with histone H1 and stimulated by chromatin-associated proteins HMG-1 and HMG-2 (2, 10, 11).

Besides functioning as an inhibitor, DFF45 is required for generating functional DFF40 nuclease. Indeed, it has not been possible to obtain catalytically active DFF40 in the absence of DFF45 (3). Interestingly, the NTDs of both DFF40 and DFF45 are indispensable in this process. Deletion of NTD from either DFF40 or DFF45 results in the production of inactive nuclease (12, 13).

In this article, we report that DFF40 NTD induces *de novo* folding of DFF45 NTD, which, by itself, is unstructured. We present the structure of the homophilic complex between NTDs of DFF40 and DFF45, which displays an extensive network of interactions across the interface. Furthermore, we discuss the implications of DFF40 and DFF45 acting as mutual chaperones for the regulation of DNA fragmentation in apoptosis.

Materials and Methods

Overproduction and Purification of His₆-Tagged DFF40 NTD (1–80), DFF45 NTD (1–116), and Chimeric gbDFF45 NTD (12–100). An NTD of human DFF40 (1–80) with a C-terminal His₆-tag was cloned into

the pET30a vector. It was expressed in the BL21(DE3) cell line, and protein production was induced with 1 mM isopropyl-D-thiogalactoside at 20°C in either LB medium (for unlabeled protein) or M9 minimal medium supplemented with [¹⁵N]NH₄Cl (1 g/liter for ¹⁵N-labeled protein) or [¹³C]glucose (2 g/liter for uniformly ¹³C-labeled protein). A quantity of 90% deuterated, uniformly ¹³C/¹⁵N-labeled protein and perdeuterated, ¹⁵N-labeled proteins was prepared by growing cells in 90% (vol/vol) D₂O supplemented with [¹⁵N]NH₄Cl and [¹³C]glucose, or 100% (vol/vol) D₂O supplemented with [¹⁵N]NH₄Cl, respectively. A 10% ¹³C-labeled sample was obtained by growing cells in M9 medium (containing 2 g/liter glucose) with 0.2 g/liter [¹³C]glucose. N-terminally His₆-tagged DFF45 NTD (1–116) was cloned into the pET15b vector and purified as described (9). Because the complex of these two constructs had very low solubility and stability, we designed a chimera in which the highly soluble streptococcal protein G B1 domain (residue 1–56) was fused to the N terminus of DFF45 NTD (residue 12–100) as a solubility enhancement tag (22). This chimera forms a 1:1 complex with DFF40 NTD, and the complex displays good quality ¹H-¹⁵N heteronuclear sequential quantum correlation (HSQC) spectra. Isotopically enriched chimeric gbDFF45 NTD (12–100) was obtained as described above.

To simplify the spectra of the complex, NMR samples were prepared in such a way that only one of the two components was isotopically enriched, and the other one was unlabeled. Cell pellets containing DFF45 and DFF40 NTDs were mixed before cell lysis and purified according to standard affinity purification protocol by using an Ni²⁺-NTA column (Qiagen, Chatsworth, CA). The eluted DFF40/45 complex was further purified to homogeneity by using gel filtration chromatography (Superdex 75, Amersham Pharmacia) and then exchanged into NMR buffer containing 20 mM phosphate (pH 6.0), 5 mM DTT, and 50 mM NaCl in H₂O/D₂O (9/1, vol/vol) or in D₂O for NMR studies.

CD Spectroscopy of DFF45 NTD (1–116) and NMR Titration

Experiments. Unlabeled DFF45 NTD (1–116) used for CD measurement was prepared as described above and was exchanged into a buffer containing 20 mM phosphate (pH 6.0) and 50 mM NaCl. The CD spectra were acquired on a Jasco J-710 spectropolarimeter (Easton, MD), averaged over four scans, and baseline-corrected. Noise reduction was performed with the manufacturer's software.

Abbreviations: NTD, N-terminal domain; CIDE, cell-death-inducing DFF45-like effector; HSQC, heteronuclear sequential quantum correlation; TROSY, transverse relaxation-optimized spectroscopy; NOESY, nuclear Overhauser effect spectroscopy.

Data deposition: The atomic coordinates and structure factors have been deposited in the Protein Data Bank, www.rcsb.org (PDB ID code 1IBX).

[§]To whom reprint requests should be addressed. E-mail: gerhard.wagner@hms.harvard.edu.

The publication costs of this article were defrayed in part by page charge payment. This article must therefore be hereby marked “advertisement” in accordance with 18 U.S.C. §1734 solely to indicate this fact.

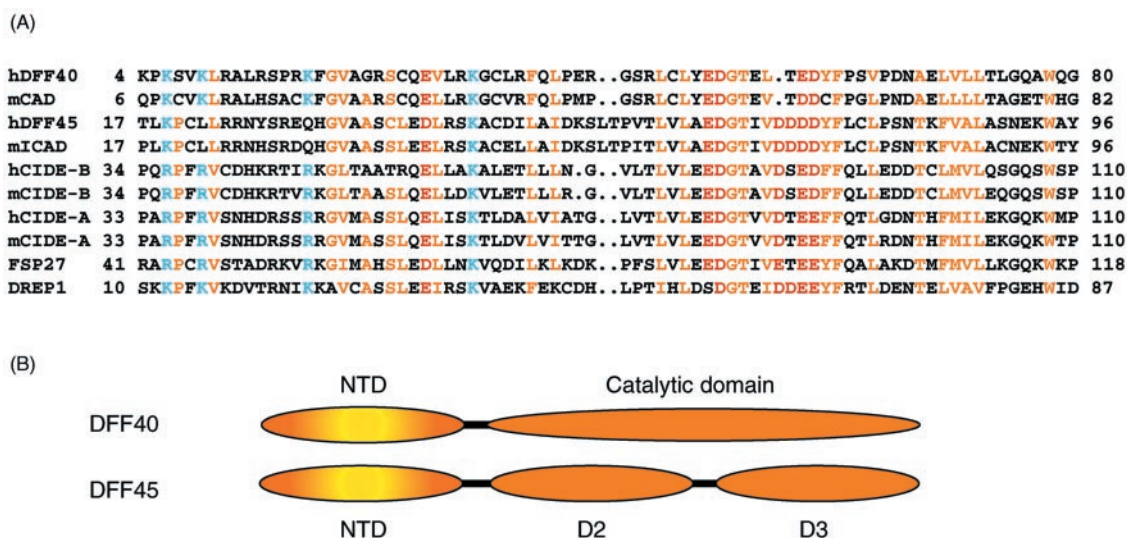


Fig. 1. (A) Sequence alignment of CIDE proteins. Residues conserved in the family are colored yellow for hydrophobic residues, blue for basic residues, and red for acidic residues. (B) Domain structures (NTD and the catalytic domain) of DFF40 and (NTD, D2, and D3) of DFF45 are shown schematically.

$^1\text{H}/^{15}\text{N}$ HSQC spectra of ^{15}N -labeled DFF45 NTD (1–116) were recorded at 23°C on a Unity 500 spectrometer (Varian), and the sample was titrated with unlabeled DFF40 NTD (1–80) at ratios of 3:1, 3:2, 1:1, 1:2, and 1:3. The spectra of ^{15}N -labeled DFF45 NTD alone and in the 1:1 complex with DFF40 are shown in Fig. 2 A and B.

NMR Spectroscopy. NMR spectra were acquired at 23°C on a Bruker Avance 500 spectrometer (Billerica, MA) equipped with a cryogenic probe, a Bruker Avance 600, or a Varian Inova 750. Sequential assignments were achieved with two pairs of triple resonance transverse relaxation-optimized spectroscopy (TROSY) experiments [TROSY-HNCA, TROSY-HN(CO)CA and TROSY-HN(CA)CB, TROSY-HN(COCA)CB] (14) by using uniformly ^{15}N - and ^{13}C -labeled 90% deuterated protein in 90% (vol/vol) $\text{H}_2\text{O}/10\%$ (vol/vol) D_2O . Side-chain proton resonances were assigned with ^{15}N -dispersed total correlation spectroscopy (TOCSY) and H(CCO)NH (15) experiments by

using a uniformly ^{15}N -labeled sample or 70% (vol/vol) deuterated ^{15}N - and ^{13}C -labeled proteins, respectively. The assignment of aromatic side chains was achieved with homonuclear TOCSY and nuclear Overhauser effect spectroscopy (NOESY) experiments acquired in D_2O by using samples with one component unlabeled and another one deuterated. Stereospecific assignments of Val and Leu protons were obtained from ^{13}C HSQC spectra by using a 10% ^{13}C -labeled sample (16). Three-bond scalar couplings $^3J_{\text{HN-HA}}$ were obtained from heteronuclear multiple quantum correlation J experiments (17).

Structural Calculation. Interproton distance constraints were derived from NOE cross-peak volumes, which were autocalibrated

Table 1. Structural statistics for the DFF40/45 CIDE complex

Measurement	Value
Nondegenerative NOE distance restraints	
All	1,665
Intra-residue	654
Sequential ($ i - j = 1$)	464
Medium-range ($ i - j \leq 4$)	161
$i, i + 2$	68
$i, i + 3$	56
$i, i + 4$	37
Long-range ($ i - j \geq 5$)	118
H bonds*	76
Dihedral angle constraints†	515
Ramachandran plot‡	
Most favorable region, %	77.0
Additionally allows region, %	22.3
Generously allowed region, %	0.7
Disallowed region, %	0.0
Average RMSD to the mean structure	
Backbone (residue 7-79 of DFF40 and 20-96 of DFF45), Å	0.39
Heavy atoms (residue 7-79 of DFF40 and 20-96 of DFF45), Å	0.84

None of these structures exhibit distance violations greater than 0.4 Å or dihedral angle violations greater than 5° .

*Hydrogen bond for α -helices was added only at the late stage of structural calculations for residues with characteristic HN(i)-Ha($i - 3$, $i - 4$) NOEs observed in the three-dimensional ^{15}N -NOESY-HSQC spectrum.

†Dihedral angle constraints were generated with DYANA (18) based on $^3J_{\text{HNH}\alpha}$ couplings, C_α chemical shifts (19), and NOE constraints.

‡PROCHECK-NMR (26) was used to assess the quality of the structures.

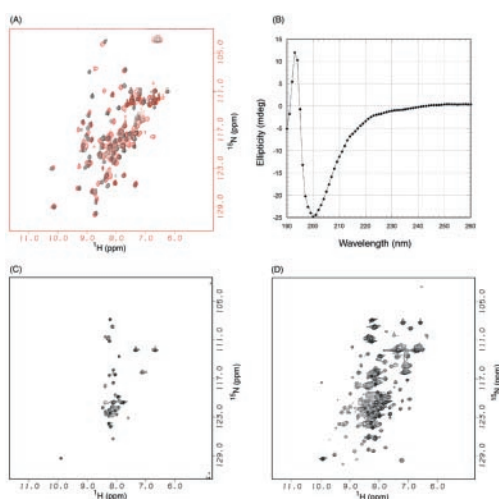


Fig. 2. DFF40 induces folding of DFF45. (A) $^1\text{H}/^{15}\text{N}$ HSQC spectra of DFF40 NTD (1–80) in the absence (black) and in the presence (red) of DFF45 NTD (1–116). (B) CD spectra of DFF45 NTD in the absence of DFF40 NTD. (C) $^1\text{H}/^{15}\text{N}$ HSQC spectra of DFF45 NTD in the absence of DFF40 NTD. (D) $^1\text{H}/^{15}\text{N}$ HSQC spectra of DFF45 NTD in the presence of DFF40 NTD.

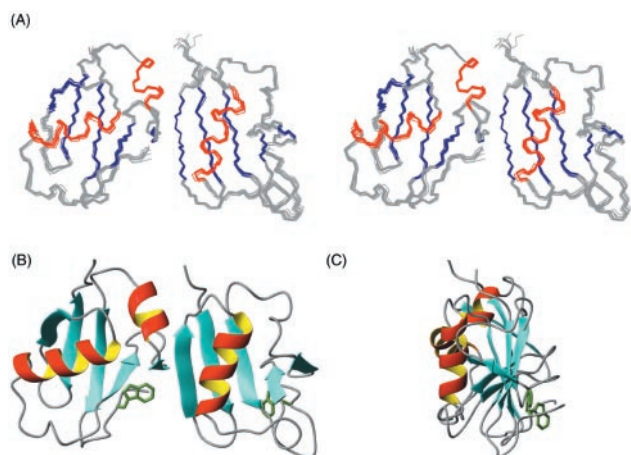


Fig. 3. Structure of DFF40/45 CIDE complex. (A) Stereo view of superimposed DFF40/45 homophilic NTD complex with DFF45 NTD (Left) and DFF40 NTD (Right). (B) Ribbon representation of the DFF40/45 NTD complex in the same orientation as A. (C) Ribbon representation of DFF40/45 complex with a 90° rotation along z axis.

with the CALIBA module from the DYANA package (18). Dihedral angle constraints were generated from $^3J_{\text{HN-HA}}$ couplings, from the chemical shift index (19), and from NOE patterns by using the HABAS program. Structures generated by the DYANA program were refined with a simulated annealing protocol in the X-PLOR program (20). Loose hydrogen-bond constraints were introduced at the late stage of structural calculation based on characteristic NOE patterns observed for α -helices or β -strands. Of the 30 calculated structures, the 10 best structures that had no NOE violations greater than 0.4 Å and no dihedral angle violations greater than 5.0° are shown in Fig. 2A. Statistics for these structures are presented in Table 1. The coordinates have been deposited in the Protein Data Bank (PDB ID no. 1IBX).

Results and Discussion

NTD of DFF40 Induces Folding of DFF45 NTD. To investigate the properties of the individual components of the complex between DFF45 and DFF40 NTDs, we recorded the $^1\text{H}/^{15}\text{N}$ HSQC spectra of DFF45 and DFF40 NTDs separately. The NTD of DFF40 displayed a well dispersed $^1\text{H}/^{15}\text{N}$ HSQC spectrum typical for structured protein (Fig. 2A, black). Titration of ^{15}N -labeled DFF40 with unlabeled DFF45 led to perturbations in the HSQC spectra in the slow exchange regime of the NMR time scale (Fig. 2A, red). In contrast, the NTD of DFF45 exhibits a spectrum typical for a disordered protein (Fig. 2C). Because nonspecific aggregation can also lead to such an appearance of the HSQC spectra, we recorded a CD spectrum of DFF45 NTD (1–116), which showed a lack of secondary structure (Fig. 2B) and confirmed that NTD of DFF45 is indeed disordered. However, this fragment of DFF45 is fully capable of inhibiting nuclease activity of DFF40 (21). Additionally, deletion of this fragment from full-length protein significantly weakens or even abolishes the chaperone potency of DFF45 (12). To reconcile these conflicting observations, we performed NMR titration of ^{15}N -labeled DFF45 NTD with unlabeled DFF40. The 1:1 complex displays well dispersed HSQC spectra (Fig. 2D), suggesting that folding of DFF45 NTD is induced upon binding to DFF40. The interaction region between the DFF45 NTD and DFF40 NTD was mapped further to residues 12–100 of DFF45 and residues 1–80 of DFF40 (data not shown).

A Solubility Enhancement Protein Tag (SET) Improves the Biochemical Property of the Complex Between DFF45 and DFF40 NTDs. Although being well structured, the complex between DFF45 and DFF40

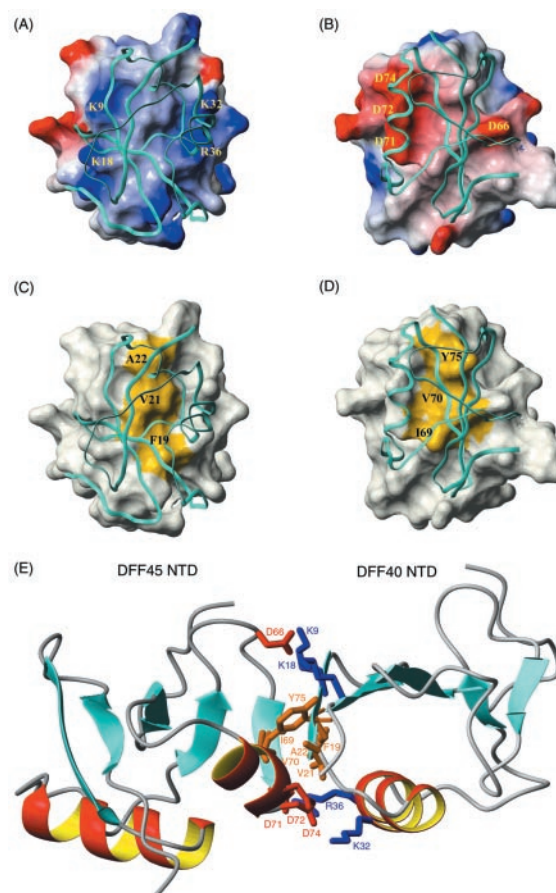


Fig. 4. Interface of the DFF40/45 CIDE complex. (A) Surface diagram of DFF40 NTD. In this figure, DFF45 NTD is shown in a ribbon diagram. The surface electrostatic potential of DFF40 is color coded so that regions with electrostatic potential $< -8 k_B T$ are red, whereas those $> +8 k_B T$ are blue (where k_B and T are Boltzmann constant and temperature, respectively). Basic residues important for the interactions are mapped on the surface. (B) Surface diagram of DFF45 NTD. In this figure, DFF40 NTD is shown in a ribbon diagram. The surface electrostatic potential of DFF45 is color coded so that regions with electrostatic potential $< -8 k_B$ are red, whereas those $> +8 k_B$ are blue (where k_B and T are Boltzmann constant and temperature, respectively). Acidic residues important for the interactions are mapped on the surface. (C) Surface diagram of DFF40 NTD (same orientation as in A). In this figure, DFF45 NTD is shown in a ribbon diagram. The hydrophobic surface of DFF40 (Phe-19, Val-21, and Ala-22) is colored yellow. (D) Surface diagram of DFF45 NTD (same orientation as in B). In this figure, DFF40 NTD is shown in a ribbon diagram. The hydrophobic surface of DFF45 (Ile-69, Val-70, and Tyr-75) is colored yellow. (E) The homophilic DFF40/45 interaction involves both hydrophilic and hydrophobic interactions. Residues involved in the binding of DFF40 and DFF45 are color coded so that hydrophobic residues are colored brown, basic residues are colored blue, and acidic residues are colored red.

NTDs exhibited poor solubility (less than 0.2 mM) and stability (precipitates within 5 days) and was not suitable for structural studies. To improve the biochemical behavior of the complex, we designed a chimeric construct in which the highly soluble B1 domain of streptococcal protein G (1–56) was N-terminally fused to residues 12–100 of DFF45 (22). An approach related to what we report here has been used successfully to screen whether bacterially expressed protein was folded without going through time-consuming purification procedures. Unlike the approach by Huth *et al.* (23), we used a nonremovable protein G B1 tag to solubilize and stabilize the NMR samples during the process of structure determination. The complex formed between DFF40 NTD (1–80) and this chimeric protein was soluble up to 0.6 mM,

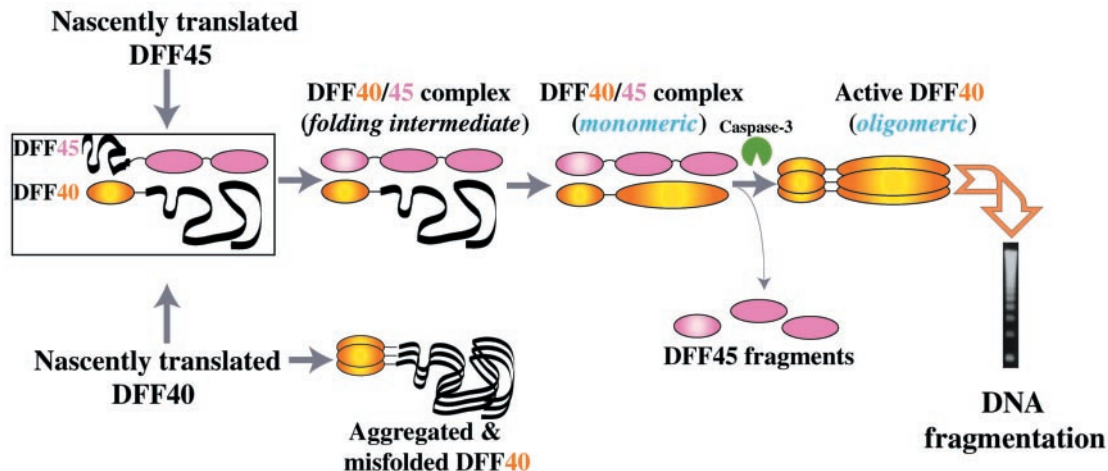


Fig. 5. Model of the mutual chaperoning of DFF40 and DFF45.

did not precipitate within 30 days, and showed high quality HSQC spectra. Importantly, the resonances of DFF45 NTD (12–100) were not affected by the introduction of the protein G B1 domain tag. Additionally, a thorough inspection of ^{15}N - and ^{13}C -dispersed NOESY spectra revealed no cross-peaks between the protein G B1 domain and DFF45 NTD (12–100) or DFF40 NTD (1–80). Based on this evidence, we concluded that the protein G B1 tag behaves as an independent structural unit and does not interfere with the formation of the DFF40/DFF45 NTD complex but enhances its solubility and stability.

Structures of DFF40 and DFF45 NTDs in the Binary Complex Are Similar to That of the NTD of CIDE-B. Shown in Fig. 3A are ten superimposed structures of the DFF40/DFF45 NTD complex. Both domains have a fold of an α/β -roll and consist of five β -strands arranged into a single β -sheet with helices packed against it, which is structurally similar to the NTD of another member of the CIDE family, CIDE-B (24). All three proteins have a prominent hydrophobic core consisting of conserved hydrophobic residues that support the packing of the helices against the β -sheet. The second hydrophobic cluster is located on the opposite side the β -sheet and is centered around a conserved Trp residue (Trp-78 in DFF40 and Trp-94 in DFF45) in the C-terminal region of the domain. Packing of this tryptophan restrains the orientation of the C-terminal loop relative to the β -sheet (Fig. 3B and C).

However, there are some significant differences among the structures of the CIDE-B, DFF40, and DFF45 NTDs. The short helix (α_2) observed in DFF45 and CIDE-B is absent in DFF40 because of the existence of two prolines in this part of the sequence. In contrast to DFF40, this helical element is preserved in the NTD of the mouse DFF40 ortholog CAD, although the structural assembly of the CAD/ICAD NTDs complex is similar to that of the human DFF40/DFF45 NTDs complex (13).

Another difference between the DFF40 and DFF45 NTDs is the packing angle of the long helix (α_1) against the β -sheet. In DFF40, α_1 forms an acute angle of $\approx 30^\circ$ with the β -strands β_1 and β_2 and is located right above them. In contrast, α_1 of DFF45 is almost perpendicular to the β -strands it packs against and, in fact, stretches over the whole β -sheet. As a result of being pushed by α_1 , α_2 of DFF45 is positioned at the far edge of β_4 to form a continuous interaction surface together with β_4 (Fig. 3B). The α_1 -helix in CIDE-B NTD is located similarly to that of DFF40, which may explain why CIDE-B NTD binds more tightly to DFF45 NTD than to DFF40 NTD (24).

The Complex Interface Buries a Central Hydrophobic Cluster Surrounded by Complementary Hydrophilic Contacts. The binding face of DFF40 NTD is primarily basic (Fig. 4A) but contains a central hydrophobic patch (Fig. 4C). In DFF45, there are primarily acidic residues that surround the hydrophobic patch on the binding surface. The complementarities of shape and charge distributions are readily visible in Fig. 4. In our previous studies, we had predicted from homology modeling a prominent polar distribution of charge residues on the surface of the DFF40 CIDE and DFF45 NTDs (24). These distinct charge distributions are indeed preserved in the DFF40/45 complex and contribute significantly to the binding interface. Basic residues from β_1 , β_2 , and α_1 (Lys-9, Lys-18, Lys-32, and Arg-36) of DFF40 form a positively charged rim surrounding a central hydrophobic convex patch formed by Phe-19, Val-21, and Ala-22 (Fig. 4A and C). Similarly, acidic residues from DFF45 (Asp-66, Asp-71, Asp-72, and Asp-74) form a negatively charged rim surrounding a central hydrophobic but concave patch formed by Ile-69, Val-70, and Tyr-75 (Fig. 4B and D). An extensive interaction network can be identified between DFF40 and DFF45. The hydrophobic cluster at the interface is formed by van der Waals contacts of Ala-22/Tyr-75, Val-21/Val-70, and Phe-19/Ile-69 from DFF40 and DFF45, respectively (Fig. 4E, central). These hydrophobic interactions are sandwiched between two areas of interactions between charged residues. A larger group involves five residues: Lys-32 and Arg-36 from DFF40, as well as Asp-71, Asp-72, and Asp-74 from DFF45 (Fig. 4E, bottom). Another group consists of three residues: Lys-9, Lys-18 from DFF40, and Asp-66 from DFF45 (Fig. 4E, top). Interestingly, all charge clusters are formed by more than one charged residue, with the exception of Asp-66. Asp-66 is in the middle of an EDG loop that is strictly conserved within the CIDE family of proteins. The point mutation of Asp-66 to Ala in the mouse DFF45 ortholog ICAD significantly weakens the DFF40/DFF45 (ICAD/CAD) interaction (13). On the other hand, point mutations of any other charged residues did not interfere with nuclease/inhibitor interaction. Only when multiple mutations resulted in the removal of the charged cluster was a pronounced interference with the complex formation observed (13). Charge–charge interactions are considered to be a driving force for providing specificity rather than affinity (25). However, in the case of the DFF40/DFF45 interaction, mutation of a single charged residue on a large charged interface does not disrupt the complex, suggesting that there is a certain degree of tolerance in the specific recognition of CIDE/CIDE complexes.

The conserved EDG loop of DFF40 (residues 50–52) may play an important role in the regulation of nuclease activity, because mutations of E50A and D51A showed diminished nuclease

activity *in vitro* (24). Our structure shows that the loop is peripheral to the main DFF40/DFF45 NTDs interaction interface but does not make direct contact with DFF45.

The DFF45 NTD Disrupts the Oligomeric State of DFF40. The mechanism of DFF40 activation is still unknown. It has been shown that the catalytic activity of DFF40 is associated with the oligomeric state of DFF40 (10). Interestingly, the DFF40/DFF45 complex is found only in the monomeric state as a heterodimeric complex with an estimated molecular mass of ≈ 85 kDa (2). Consistent with this observation, the homophilic complex between DFF40 and DFF45 NTDs exists predominantly in a monomeric state in solution. However, when DFF45 NTD is absent, the regulatory domain of DFF40 oligomerizes and elutes from the gel filtration column in fractions of molecular mass larger than 80 kDa (data not shown). A similar effect was also observed for CAD (the mouse ortholog of DFF40), which undergoes aggregation under physiological pH at NMR concentrations (13). Thus, the regulatory NTD of DFF40 may also serve as an oligomerization domain, once DFF45 NTD is removed. Therefore, the NTD of DFF40 may possess three functions and serve as a DFF45-interaction domain, an oligomerization domain in the absence of DFF45, and finally, an activation domain (24). All these roles are important for the transition between the dormant and active states of DFF40 nuclease and, therefore, are crucial for the regulation of DNA fragmentation in apoptosis.

Conclusions

DFF45 has been characterized as an inhibitor and chaperone of DFF40 (2, 3). In this study, we demonstrate that, in fact, DFF40 and DFF45 function as mutual chaperones. Binding of the regulatory NTD of DFF40 induces proper folding of the corresponding domain of DFF45. *De novo* folded DFF45 subsequently chaperones the catalytic domain of DFF40 (3). Thus, the regulation of equal production of folded nuclease DFF40 and its

inhibitor DFF45 is achieved through multiple transitions between different folding and association states of the proteins (Fig. 5). The maintenance of a 1:1 ratio of these molecules might be important for the homeostasis of normal cells, because an excess of DFF45 will increase the threshold for downstream apoptotic signaling, whereas an overproduction of DFF40 will result in irreparable DNA damage. Such an interpretation should be treated with caution, however, because *in vitro* experiments may not reflect *in vivo* processes completely.

Additionally, we present the solution structure of the complex between the NTDs of DFF40 and DFF45. Individual domains assume the α/β -roll fold similar to the structure of the NTD of CIDE-B. DFF40 and DFF45 NTDs display a distinct way of helix packing, which results in the formation of specific binding interfaces. It consists of a convex surface region of DFF40 in which basic residues surround a hydrophobic patch and a concave surface of DFF45 with acidic residues centered around an apolar region. A combination of hydrophilic and hydrophobic interactions contributes to the formation of this complex and determines the specificity of the interaction. The DFF40-initiated folding of DFF45 apparently causes a reduction of the affinity while maintaining specificity. The reduced affinity may be crucial for the activation of DFF40, which requires a dissociation of the complex upon caspase cleavage of DFF45. This unique way of macromolecular recognition serves as a specificity filter in the regulation of DNA fragmentation in apoptosis.

We thank Dr. John Gross and Mr. Gregory Heffron for productive discussions of the TROSY pulse sequences and help with the use of the spectrometers. This research was supported in part by Grant GM38608 from the National Institutes of Health (to G.W.). Acquisition and maintenance of spectrometers and computers used for this work were supported by the National Science Foundation (Grant MCB 9527181), the Harvard Center for Structural Biology, and the Giovanni Armenise-Harvard Foundation for Advanced Scientific Research. P.L. was funded by the National Science and Technology Board of Singapore.

1. Thompson, C. B. (1995) *Science* **267**, 1456–1462.
2. Liu, X., Li, P., Widlak, P., Zou, H., Luo, X., Garrard, W. T. & Wang, X. (1998) *Proc. Natl. Acad. Sci. USA* **95**, 8461–8466.
3. Enari, M., Sakahira, H., Yokoyama, H., Okawa, K., Iwamatsu, A. & Nagata, S. (1998) *Nature (London)* **391**, 43–50.
4. Sakahira, H., Enari, M. & Nagata, S. (1998) *Nature (London)* **391**, 96–99.
5. Halenbeck, R., MacDonald, H., Roulston, A., Chen, T. T., Conroy, L. & Williams, L. T. (1998) *Curr. Biol.* **8**, 537–540.
6. Inohara, N., Koseki, T., Chen, S., Wu, X. & Nunez, G. (1998) *EMBO J.* **17**, 2526–2533.
7. Aravind, L., Dixit, V. M. & Koonin, E. V. (1999) *Trends Biochem. Sci.* **24**, 47–53.
8. Mukae, N., Enari, M., Sakahira, H., Fukuda, Y., Inazawa, J., Toh, H. & Nagata, S. (1998) *Proc. Natl. Acad. Sci. USA* **95**, 9123–9128.
9. McCarty, J. S., Toh, S. Y. & Li, P. (1999) *Biochem. Biophys. Res. Commun.* **264**, 181–185.
10. Liu, X., Zou, H., Widlak, P., Garrard, W. & Wang, X. (1999) *J. Biol. Chem.* **274**, 13836–13840.
11. Toh, S. Y., Wang, X. & Li, P. (1998) *Biochem. Biophys. Res. Commun.* **250**, 598–601.
12. Gu, J., Dong, R. P., Zhang, C., McLaughlin, D. F., Wu, M. X. & Schlossman, S. F. (1999) *J. Biol. Chem.* **274**, 20759–20762.
13. Otomo, T., Sakahira, H., Uegaki, K., Nagata, S. & Yamazaki, T. (2000) *Nat. Struct. Biol.* **7**, 658–662.
14. Salzmann, M., Wider, G., Pervushin, K., Senn, H. & Wuthrich, K. (1999) *J. Am. Chem. Soc.* **121**, 844–848.
15. Lin, Y. & Wagner, G. (1999) *J. Biomol. NMR* **15**, 227–239.
16. Szyperski, T., Neri, D., Leiting, B., Otting, G. & Wuthrich, K. (1992) *J. Biomol. NMR* **2**, 323–334.
17. Bax, A., Griffey, R. H. & Hawkins, B. L. (1983) *J. Magn. Reson.* **55**, 301–305.
18. Guntert, P., Mumenthaler, C. & Wuthrich, K. (1997) *J. Mol. Biol.* **273**, 283–298.
19. Wishart, D. S. & Sykes, B. D. (1994) *J. Biomol. NMR* **4**, 171–180.
20. Brünger, T. A. (1994) X-PLOR Manual 3.851: A System for X-ray Crystallography and NMR (Yale Univ. Press, New Haven, CT).
21. McCarty, J. S., Toh, S. Y. & Li, P. (1999) *Biochem. Biophys. Res. Commun.* **264**, 176–180.
22. Zhou, P., Lugovskoy, A. A. & Wagner, G. (2001) *J. Biomol. NMR*, in press.
23. Huth, J. R., Bewley, C. A., Jackson, B. M., Hinnebusch, A. G., Clore, G. M. & Groneborn, A. M. (1997) *Protein Sci.* **6**, 2359–2364.
24. Lugovskoy, A. A., Zhou, P., Chou, J. J., McCarty, J. S., Li, P. & Wagner, G. (1999) *Cell* **99**, 747–755.
25. DeLano, W. L., Ultsch, M. H., de Vos, A. M. & Wells, J. A. (2000) *Science* **287**, 1279–1283.
26. Laskowski, R. A., MacArthur, M. W., Moss, D. S. & Thornton, J. M. (1993) *J. Appl. Crystallogr.* **26**, 283–291.